Available online at www.sciencedirect.com
ScienceDirect
Trans. Nonferrous Met. Soc. China 33(2023) 683−700
Transactions of Nonferrous Metals Society of China
www.tnmsc.cn

Mechanical properties, impact initiation characteristics and energy release effect of Al/PTFE reactive materials enhanced by Fe particles

Xiang-chun XU[1], Qing-chun ZHANG[2], Hong-jie FANG[1,3], Bao-yue GUO[4], Wen LIANG[4], Bo JIN[2], Ru-fang PENG[2], Kun YU[1], Rong CHEN[4]

1. School of Materials Science and Engineering, Central South University, Changsha 410083, China;
2. State Key Laboratory of Environment-friendly Energy Materials, Southwest University of Science and Technology, Mianyang 621010, China;
3. College of Materials Science and Engineering, Yantai Nanshan University, Yantai 265713, China;
4. College of Sciences, National University of Defense Technology, Changsha 410008, China

Received 29 October 2021; accepted 31 March 2022

Abstract: Aluminum/polytetrafluoroethylene (Al/PTFE) composites are a promising category of reactive structural materials. In order to improve the mechanical properties and reactivity, Fe particles were introduced into Al/PTFE. Quasi-static and dynamic compression tests for Al/PTFE/Fe reactive materials were conducted, and significant strain and strain rate hardening phenomena were observed. The compression strength of Al/PTFE with Fe content of 30 wt.% reached 191.8 MPa at the strain rate of 5000 s^{-1}, increased by 39% compared to Al/PTFE. The oriented PTFE nano-fibers could effectively prevent the propagation of micro-cracks. The impact reaction processes under SHPB and drop-weight conditions were observed by high-speed photography technology, and the reactivity was qualitatively characterized by a newly-designed device. Based on the results of TG-DSC and XRD analyses, the reaction involving Al/PTFE and Al/Fe was clarified. The Johnson−Cook constitutive model was established and the model results agreed well with experimental data. Under impact loading, the reactivity was speculated to be the result of multiple actions.

Key words: reactive materials; Al/PTFE/Fe; mechanical behavior; energy release characteristics; impact initiation mechanism

1 Introduction

Reactive structure materials (RSMs) are a special category of energetic composites which integrate mechanical strength and high energy density [1]. Generally, RSMs consist of two or more non-reactive solid materials, such as intermetallic, metal/polymer, metal hydride/polymer, and thermites. They stay inert and insensitive under normal conditions, but react violently under intense impact or high strain-rate loading, releasing a large amount of chemical energy. Due to their excellent mechanical properties and energetic characteristics, metal/polymer composites are widely used in military and civilian applications to replace traditional inert units such as reactive fragments, anti-missile warheads and oil-well perforation. Al/PTFE is a typical metal/polymer energetic composite which has sufficient mechanical strength and inertness to meet the needs of transportation and launch, and can generate high temperature (pressure) and release considerable chemical energy when subjected to high-speed impact. Therefore,

Corresponding author: Kun YU, Tel: +86-13975808242, E-mail: yukun2010@csu.edu.cn;
Rong CHEN, Tel: +86-15111054757, E-mail: r_chen@nudt.edu.cn
DOI: 10.1016/S1003-6326(22)66138-7
1003-6326/© 2023 The Nonferrous Metals Society of China. Published by Elsevier Ltd & Science Press

Al/PTFE reactive materials have received widespread attention.

Over the past decades, many researchers have made notable progress in the formulation, preparation process, impact-initiation reaction mechanism and numerical modeling of Al/PTFE composites. FENG et al [2,3] found that the sintering temperature, mass ratio and Al particle size influenced the compressive strength and reaction sensitivity of Al/PTFE. A series of Al/PTFE specimens [4] with different molding pressures were prepared, and impact loading was conducted by SHPB. The results showed that initial defects inside the specimen could effectively reduce the ignition threshold. However, traditional Al/PTFE reactive materials have relatively low density and mechanical strength. In order to meet the actual application requirements, W powder (19.3 g/cm^3) is usually added into Al/PTFE to improve its mechanical properties [5]. WANG et al [6] found that with the increase in content of W, the quasi-static compressive strength did not change significantly, but the dynamic compressive strength increased to 132 MPa at the W content of 80%. XU et al [7] studied the quasi-static compression properties of Al/PTFE/W samples before and after sintering, and found that the sintered specimens showed obvious strain strengthening effect. CAI et al [8] found that under the same mass ratio, a relatively high ultimate compression strength was observed in Al/PTFE/W composites with fine W particles despite higher porosity. This phenomenon may be attributed to the formation of mesoscale force chains between metal particles. HERBOLD et al [9] confirmed that by numerical modeling force chains are easier to form among fine metal particles, which in turn lead to an increase in ultimate compression strength.

Although adding W to Al/PTFE can greatly improve its mechanical behavior, the low reaction heat between PTFE and W (0.47 kJ/g) would inevitably reduce the damage ability. Thus, many researchers have tried to add other strengthening phases to improve both mechanical properties and reaction heat. WANG et al [10] added Ni into Al/PTFE and achieved dynamic compressive strength as high as 130 MPa at the strain rate of 3000 s^{-1}. Moreover, a bilinear relationship was observed between stress and log ε. YU et al [11] introduced ZrH_2 into Al/PTFE and found that the compression strength reached a maximum of 112.7 MPa when ZrH_2 content was 5%. Besides, special flames were observed, which denoted the reaction between ZrH_2 and PTFE. In another study, Al_2O_3 and SiC were added into Al/PTFE [12], and it was found that the mechanical strengthening effect of SiC was more obvious than that of Al_2O_3. DING et al [13] added CuO into Al/PTFE to investigate the influence of particle size and mass ratio on energy release ability. The energy release ability with Al/CuO content of 50% was 3.35 times higher than that of Al/PTFE and the energy release rate was as high as 63.63%.

In order to improve the penetration ability of Al/PTFE reactive structural materials, it is necessary to ensure a certain density and mechanical strength without losing the reaction heat. Therefore, in this study, iron (Fe) powder was added as reinforcement into Al/PTFE for the first time. Fe powder has a relatively high density (7.87 g/cm^3). Al and Fe can undergo an intermetallic reaction, releasing a large amount of reaction heat [14,15]. Hence, six kinds of specimens with different Fe contents were fabricated. Quasi-static and dynamic compression tests were conducted to explore the mechanical response at different strain rates. Moreover, fractured surfaces were observed by SEM and the Johnson−Cook constitutive model was established. Impact sensitivity tests were conducted, the energy release effect was quantitatively characterized by improved drop-weight device, and the impact reaction processes were recorded by high-speed camera. Based on both TG−DSC and XRD analyses, the reaction mechanism was clarified. In this research, the mechanical properties, impact reaction characteristics and initiation mechanism of Al/PTFE with different Fe contents were investigated, which may provide a reference for the formulation, design and application.

2 Experimental

2.1 Raw materials and specimens preparation

The starting powders used to fabricate the specimens have the following average particle sizes: Al 20 μm, Fe 20 μm, and PTFE 25 μm. In order to obtain the maximum reaction heat, Al/PTFE was selected as independent unit, which was mixed in accordance with the chemical equilibrium ratio

(Al:PTFE=26.5 wt.%:73.5 wt.%). The mass fraction of Fe powder ranged from 10% to 50% of the total mass. Al/PTFE without Fe was prepared as the control sample. The mass fraction of Al, PTFE and Fe, and the corresponding theoretical maximum density (TMD) are listed in Table 1.

Table 1 Composition and theoretical maximum density of Al/PTFE/Fe specimens

Type	Mass fraction/%			TMD/(g·cm^{-3})
	Al	PTFE	Fe	
A	26.5	73.5	0	2.31
B	23.4	66.6	10	2.49
C	20.8	59.2	20	2.69
D	18.2	51.8	30	2.93
E	15.6	44.4	40	3.22
F	13.0	37.0	50	3.58

The preparation process [16] involved mixing, drying, cold isostatic pressing and vacuum sintering. First, the raw powders were weighed proportionally, and appropriate amount of absolute ethanol was added. Then, the mixture was stirred by electric mixer and the resulting suspension was placed in a vacuum oven. After that, the dried powder was placed in a cylindrical mold and cold-pressed under the pressure of 300 MPa to obtain the cylindrical specimens. Finally, the specimens were placed in a vacuum sintering oven at 360 ℃ for 5 h [17].

2.2 Methods

2.2.1 Microstructure characterization

The internal microstructure and fractured surfaces were observed using scanning electron microscope (SEM, Quanta 200). The sintered specimens were analyzed by X-ray diffraction (XRD, DMAX−2500×), which covered the 2θ range of 10°−90° at a scanning speed of 6 (°)/min.

2.2.2 Quasi-static compression tests

Quasi-static compression tests were conducted using a Universal Materials Testing Machine (MTS 810). The specimens were compressed at a constant speed of 2 mm/min, which corresponded to a nominal strain rate of 1×10^{-3} s^{-1}.

2.2.3 Dynamic compression tests

Dynamic compression tests were carried out by a Split-Hopkinson pressure bar (SHPB) system. A schematic diagram of the device is shown in Fig. 1. The bars were all LC4 aluminum bars. The test sample with size of d6 mm × 3 mm was sandwiched between the incident bar and transmitted bar. Based on the strain pulse signals obtained from the strain gauge, the stress−strain curves and strain rate were obtained. A high-speed camera with the frame rate of 20000 frames per second was used to record the compression deformation and reaction process.

2.2.4 Drop-weight tests and qualitative characterization of reactivity

The impact sensitivity of Al/PTFE/Fe reactive materials was tested by a standard drop-weight device. Twenty specimens of each type with size of d10 mm × 3 mm were tested and the impact sensitivity was calculated by characteristic drop height (H_{50}), at which the specimens have a 50% probability of reaction. The testing method is based on the "up-and-down" technique [18], and the calculation formula is as follows:

$$H_{50}=\left[A+B\left(\frac{\sum iN_i}{N}-\frac{1}{2}\right)\right] \quad (1)$$

where A is the initial height, B is the height interval, i is the order of height sequence from 0, N_i is the number of reaction events at a certain height, and N is the total number of reaction events.

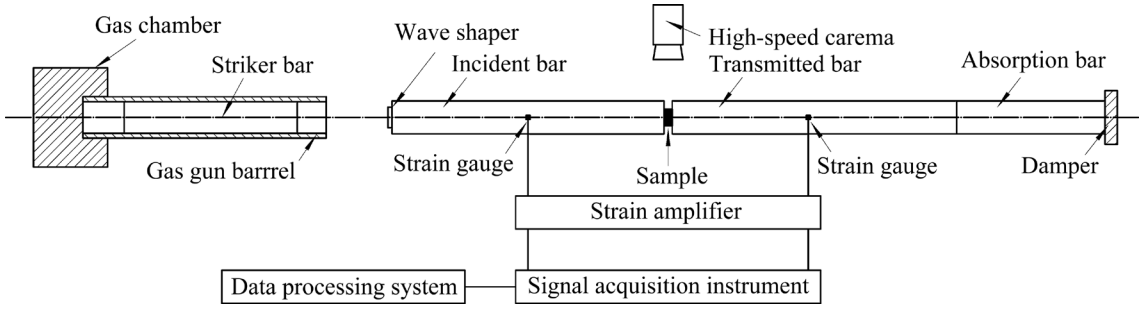

Fig. 1 Schematic diagram of SHPB experiment device

DING et al [13] designed an energy release device based on the report by AMES [19] using a standard drop-weight, which can qualitatively characterize the reactivity. Hence, this energy release device was used and its layout is shown in Fig. 2. The working principle of the device is as follows. The sample is sandwiched between impact plunger and bottom plate. The drop-weight falls freely and hits the impact plunger, which further strikes the specimen and initiates the reaction. Due to the violent explosion, the air in the chamber expands rapidly, forming high-pressure gas which pushes the piston pipe outward. A plastic board with coordinate grid paper was placed perpendicular to the high-speed camera and was used together to record the displacement−time curves of the piston. The pressure sensor placed on the back wall of the chamber simultaneously records the pressure−time curves. Combining these two complementary results, the energy release effect can be more accurately characterized through qualitative analysis.

2.2.5 TG-DSC tests

The thermal reaction process was investigated using a thermogravimetry-differential scanning calorimetry simultaneous thermal analyzer (TG-DSC, NETZSCH-STA449C). The tests were conducted under argon atmosphere, and the specimens were heated to 800 ℃ at a heating rate of 15 ℃/min.

3 Results and discussion

3.1 Microstructure

The internal microstructures of Al/PTFE/Fe composites are shown in Fig. 3. The microstructure characteristics of Type B before and after sintering are compared, as shown in Figs. 3(a, b). Before sintering, there were numerous pores existing between metal particles and PTFE matrix, the components were arranged loosely, and metal particles were exposed outside the matrix. By comparison, Fig. 3(b) demonstrates that PTFE formed a dense and continuous matrix in which the metal particles were embedded tightly, and particles were distributed evenly and discretely. In this regard, during sintering process, the crystalline PTFE turned into amorphous state, the movement of viscous PTFE molecules intensified [3], and the interface between the PTFE particles disappeared. Consequently, PTFE wrapped the metal particles and fused together to make it a dense and homogeneous whole.

Figures 3(b−f) show the internal micro-structural characteristics of Types B−F after sintering. It can be seen that Al and Fe particles were surrounded by the continuous PTFE matrix. The Fe particles appeared brighter compared with Al particles due to their higher atomic number. As shown in Figs. 3(b−d), when the metal particle contents were relatively low, the harder metal particles exerted a certain strengthening effect on the matrix. However, excessive Fe particles can destroy the continuity and integrity of the matrix, as observed in Figs. 3(e, f). In addition, Al and Fe metal particles formed a few interstitial pores due to non-dense pile up during the cold pressing process, which finally remained in the sintered specimens [20,21].

3.2 Quasi-static compression properties of Al/PTFE/Fe specimens

3.2.1 Quasi-static compression results

Taking the experiment results of Type C as an example, it was found that the true stress−strain

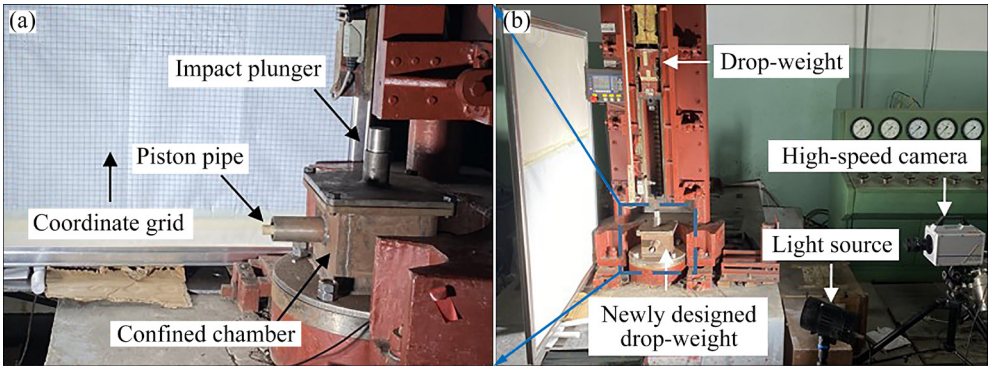

Fig. 2 Improved energy release device (a) and layout of drop-weight device (b)

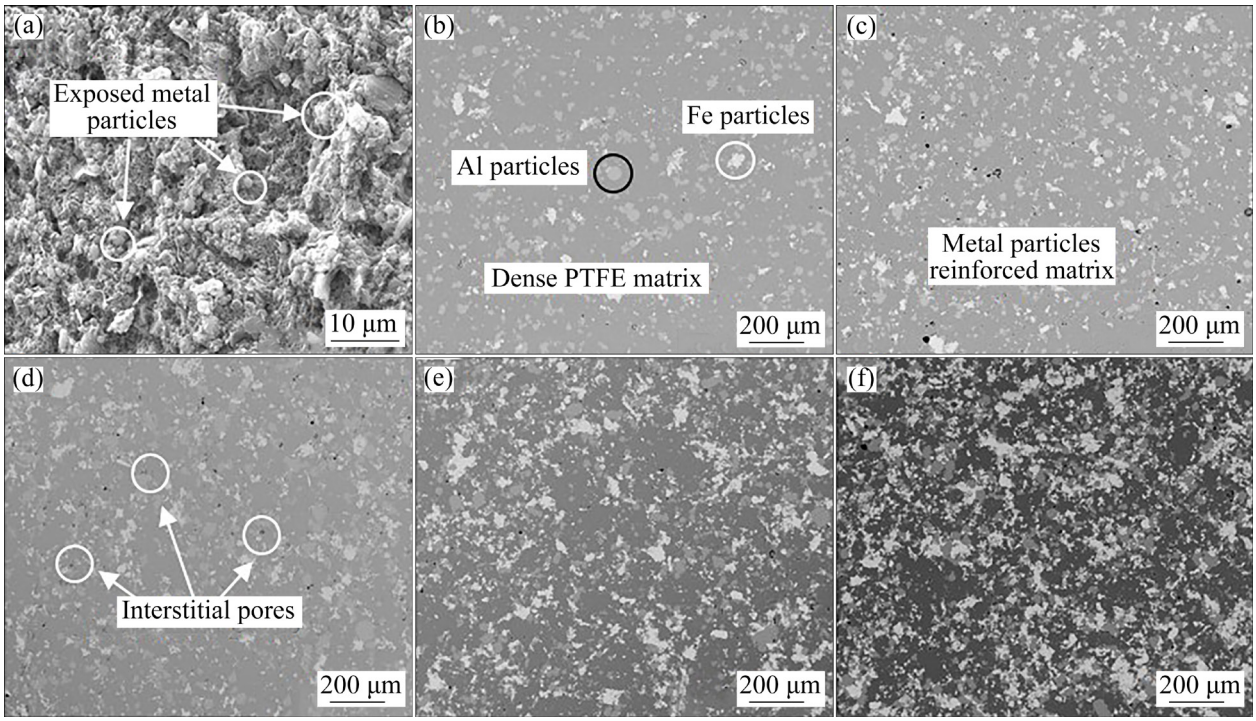

Fig. 3 Interior microstructures of Al/PTFE/Fe specimens: (a) Unsintered specimens of Type B; (b−f) Sintered specimens of Types B−F, respectively

curves of the triplicate parallel experiments almost overlapped together, as shown in Fig. 4(a), which indicates good reliability and repeatability of the experimental results.

The true stress−strain curves of Al/PTFE/Fe specimens are shown in Fig. 4(b), and their corresponding mechanical parameters are listed in Table 2. It can be observed that the specimens were all elastoplastic materials, which first went through a short linear elastic stage, reaching the yield point, and then underwent plastic deformation. Significant strain hardening phenomenon was observed. Subsequently, the relatively weak PTFE matrix fractured and the specimen failed. The compression strength increased first and then decreased with the increase in Fe content. When Fe content was 30%, the compression strength reached the maximum of 108.5 MPa, which increased by 47.2% compared to Al/PTFE. However, when the Fe content was higher than 30%, the compression strength showed a downward trend. When Fe content was 50%, the compression strength was still 79.54 MPa, slightly higher than that of Al/PTFE. According to the results, adding Fe powder to Al/PTFE had a significant strengthening effect on the mechanical properties.

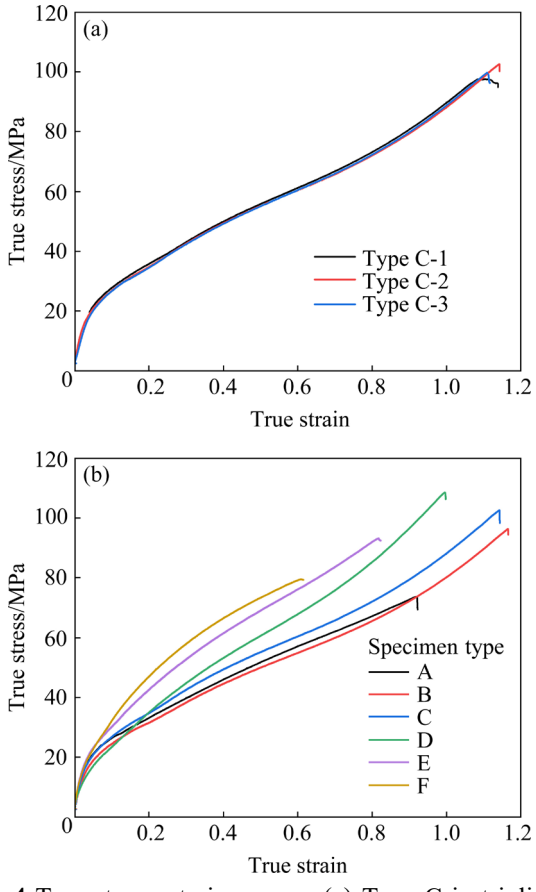

Fig. 4 True stress−strain curves: (a) Type C in triplicate parallel experiments; (b) Six types of specimens under quasi-static compression

3.2.2 Fracture and reinforcement mechanism by SEM

Al/PTFE/Fe reactive materials are typical particle-reinforced composites [22] whose mechanical strength mainly depends on the PTFE matrix and the interfaces between the metal particles and polymers. SEM analysis was carried out on the fracture surfaces in order to explore the fracture and reinforcement mechanism, as shown in Fig. 5. In the elastic deformation stage, the deformation was mainly concentrated on the crystalline PTFE matrix, and the process was reversible. Since metal particles have both higher hardness and compressive strength than PTFE matrix [23], they could bear more stress loading under the same strain during plastic deformation. Besides, the "softer" matrix and "harder" discontinuous phase combined to enhance the shear failure stress [24]. Thus, when Fe content increased to 30%, the compression strength increased monotonically. As the loading proceeded, the specimens were gradually pressed into flat shapes, which bore compressive stress in the axial direction and at the same time, bore tensile stress in the radial direction. Under circumferential tensile stress, mode-I open cracks appeared [25], as shown in Fig. 5(a). Due to the inhomogeneity of bonding strength at the interfaces between metal particles and PTFE matrix, metal particles began to slip against each other (Fig. 5(b)) and the filled metal particles were pulled out of the matrix, resulting in "de-bonding" of metal particles from polymers (Fig. 5(c)). At the same time, micro-cracks occurred and gradually grew into macro-cracks. Finally, the relatively weak PTFE matrix fractured, and the specimen failed.

However, numerous PTFE nano-fibers were also observed on the fracture surface, as shown in Fig. 5(e). BROWN and DATTELBAUM [26] reported that PTFE fibers usually nucleated at the position of stress concentration due to the shear localization. KITAMURA et al [27] found that the softening effect was caused by plastic deformation, and a large amount of oriented PTFE fibrils formed in the direction of loading. As shown in Figs. 5(f–h), the fibers were usually linked to the fractured

Table 2 Mechanical properties of Al/PTFE/Fe specimens under quasi-static compression

Type	Elastic modulus/MPa	Yield strength/MPa	Hardening modulus/MPa	Compression Strength/MPa	Failure strain
A	491.8	20.5	56.5	73.7	0.91
B	502.1	21.7	59.9	96.3	1.16
C	566.3	22.1	64.3	102.5	1.14
D	564.2	22.5	84.8	108.5	0.99
E	560.1	20.9	78.2	93.2	0.82
F	528.7	19.9	67.5	79.5	0.61

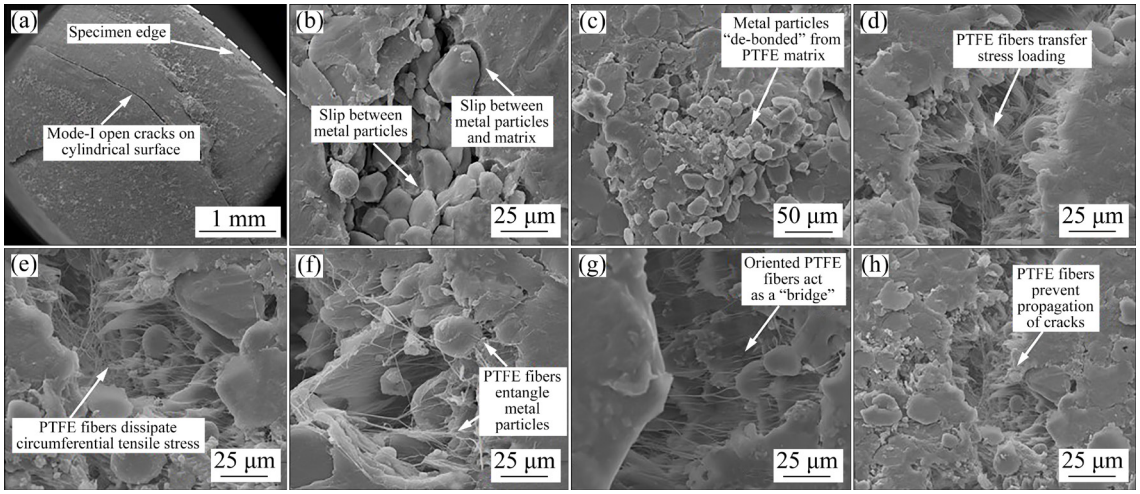

Fig. 5 Microstructure of fracture surfaces of Al/PTFE/Fe specimens

surfaces between two opposite sides of the matrix, which also entangled and wrapped metal particles to hinder slip. Due to the elasticity of PTFE fibers, oriented fibers were able to transfer the stress loading and generate a certain resilience to make the matrix closer [28]. Moreover, they acted as "a bridge" to provide additional resistance to prevent the growth of initial micro-cracks and propagation of macro-cracks [29], which may be another important mechanical reinforcement mechanism.

When the Fe content exceeded 30%, metal particles were more prone to slip because of relatively low content of polymer, leading to premature failure at low strain rates. Also, additional metal particles destroyed the continuity and integrity of PTFE matrix, as shown in Fig. 3(f), leading to the decrease in compression strength.

3.3 SHPB dynamic compression

3.3.1 Dynamic compression results

The signal−time curves and stress-state equilibrium curves of Type C sample are shown in Fig. 6. Three samples of each type at identical strain rate were tested to ensure the consistency. The true stress−strain curves of six kinds of specimens at different strain rates are shown in Fig. 7, and the corresponding dynamic compression properties are listed in Table 3.

Similar to the compression deformation behavior under quasi-static conditions, dynamic mechanical response of Al/PTFE/Fe specimens could be divided into four stages: elastic deformation, plastic deformation, failure and impact-initiation reaction. Significant strain hardening and strain rate hardening phenomena were observed in all types of specimens. Both yield and compression strengths were improved with increase in strain rate. With the increase in Fe content, yield and compression strength increased first and then decreased at identical strain rate. At the strain rate of 5000 s^{-1}, with Fe content of 30%, the compression strength was 191.8 MPa, which was improved by 39% compared to Al/PTFE. It is also worth noting that when the Fe content was 30%, the compression strength was increased by 77% compared to quasi-static compression condition. When the Fe content exceeded 30%, the dynamic compression strength decreased because

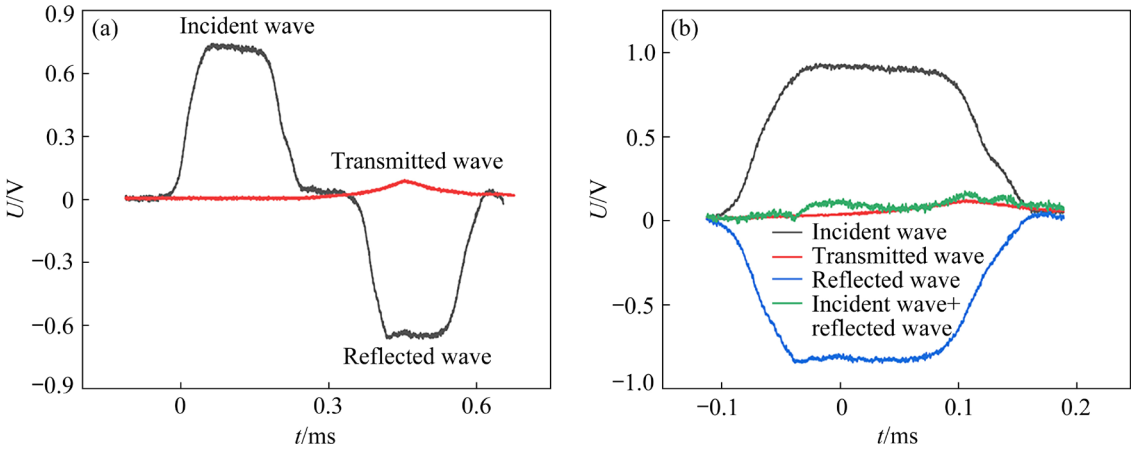

Fig. 6 Signal−time curves (a) and stress-state equilibrium curves (b) of Type C specimen

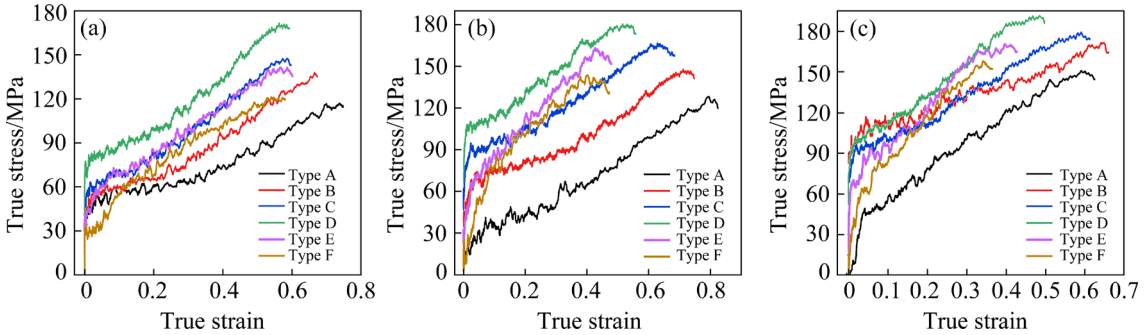

Fig. 7 True stress−strain curves of six types of specimens under dynamic compression tests at different strain rates: (a) 3000 s^{-1}; (b) 4000 s^{-1}; (c) 5000 s^{-1}

Table 3 Mechanical properties of Al/PTFE/Fe specimens under dynamic compression tests at different strain rates

Type	Strain rate/s^{-1}	Elastic modulus/MPa	Yield strength/ MPa	Hardening modulus/MPa	Compression strength/MPa	Failure strain	Strain energy/ ($J·cm^{-3}$)
A	3000	2015.2	38.9	90.9	117.1	0.79	61.2
	4000	2809.1	42.1	135.6	128.2	0.74	
	5000	3677.2	48.7	175.5	138.3	0.64	
B	3000	2102.5	48.4	126.8	137.8	0.71	82.3
	4000	2857.3	66.7	138.5	147.8	0.67	
	5000	3642.1	89.9	181.2	174.6	0.60	
C	3000	2123.6	55.1	149.3	147.7	0.63	89.1
	4000	2897.2	92.2	158.1	166.6	0.58	
	5000	3654.5	94.8	170.2	179.6	0.57	
D	3000	2133.5	76.5	164.9	171.0	0.57	91.2
	4000	2901.2	104.4	172.5	180.4	0.52	
	5000	3685.2	105.8	230.1	191.9	0.49	
E	3000	2122.3	39.2	159.6	144.6	0.54	54.1
	4000	2854.3	40.2	160.1	162.9	0.43	
	5000	3658.1	68.7	171.2	170.8	0.39	
F	3000	2105.7	28.3	146.5	121.4	0.53	39.6
	4000	2831.2	30.8	150.2	143.6	0.40	
	5000	3642.3	62.8	162.1	158.1	0.34	

the continuity of PTFE matrix was destroyed and the slip between metal particles intensified. When Fe content was 50%, dynamic compression strength at elevated strain rates ranging from 3×10^3 to 5×10^3 s^{-1} was higher than that of Al/PTFE, which indicated that Fe particles had a remarkable strengthening effect on Al/PTFE. However, at the same strain rate, when Fe content increased, the failure strain decreased monotonically, which was different from that under quasi-static compression.

3.3.2 Impact-initiation reaction process analysis

Generally, when impacted at a certain strain rate, reactive materials would initiate and react violently accompanied by bright firelight and black smog. When subjected to impact loading, the impact and reaction processes can be typically divided into four stages. In the first stage, when the stress wave propagated from the incident bar to the specimen, the sample started to be compressed and deformed within 0−100 μs, as shown in Figs. 8(a, b). Soon after the plastic deformation (Fig. 8(c)), micro-cracks formed and propagated. Some tiny fragments were extruded out of the pressure bars, and local discrete fire and light were observed, which demonstrated that chemical reaction was triggered (Fig. 8(d)). After the specimen was destroyed completely, discrete fire suddenly became more intense and brighter, and grew towards the direction of stress propagation (Figs. 8(e, f)). During this stage, the rapidly spreading fire and hot-spots induced more broken fragments to participate in the reaction and sustain the reaction. Thus, a larger scale deflagration was observed and the growth of fire formed a mushroom-like shape (Fig. 8(g)), accompanied by black smoke and a deafening sound. The reaction usually lasted thousands of microseconds (Figs. 8(d−j)). At the final stage, the fire gradually extinguished, and only some unreacted fragments were ejected along the loading direction (Figs. 8(k, l)).

3.3.3 Effect of Fe content

Dynamic compression strength and toughness are generally determined by the mass ratio of the composites, and play a vital role in impact-initiation reaction [30]. The impact reaction processes of different types of composites at the same strain rate of 5000 s^{-1} are compared in Fig. 9.

As can be seen from Fig. 9(a), Type A had longer ignition delay time and its reaction was weaker. Only sporadic flames were observed and no intense firelight was generated until the end of reaction. Upon compression, Type C reacted suddenly after the specimen was broken, the flame spread rapidly after initiation, and became more intense and gathered into a light-ball. There were hardly any unreacted fragments after impact. Furthermore, Type F did not react at all. Instead, the specimen underwent deformation, and numerous debris splashed and flew away along the loading direction, but no ignition occurred. Combined with recorded photographs and the true stress−strain curves in Fig. 7(c), it can be concluded that the reactivity was closely related to the mechanical properties [25]. Hence, the specimen with higher compression strength had shorter ignition delay time and more intense reaction process.

FENG et al [2,3] considered that the initiation of reaction is more likely to occur in a mechano-chemical manner rather than a thermochemical manner. During dynamic impact, the specimen absorbed the mechanical work from the pressure bars, and converted it into internal chemical energy. Localized regions underwent rapid or large plastic deformation, which in turn generated hot-spots and spread through the whole sample. The mechano-chemical process could be considered adiabatic due to its extremely short occurrence time. The mechanical work absorbed by the specimen from impact loading per unit volume can be calculated

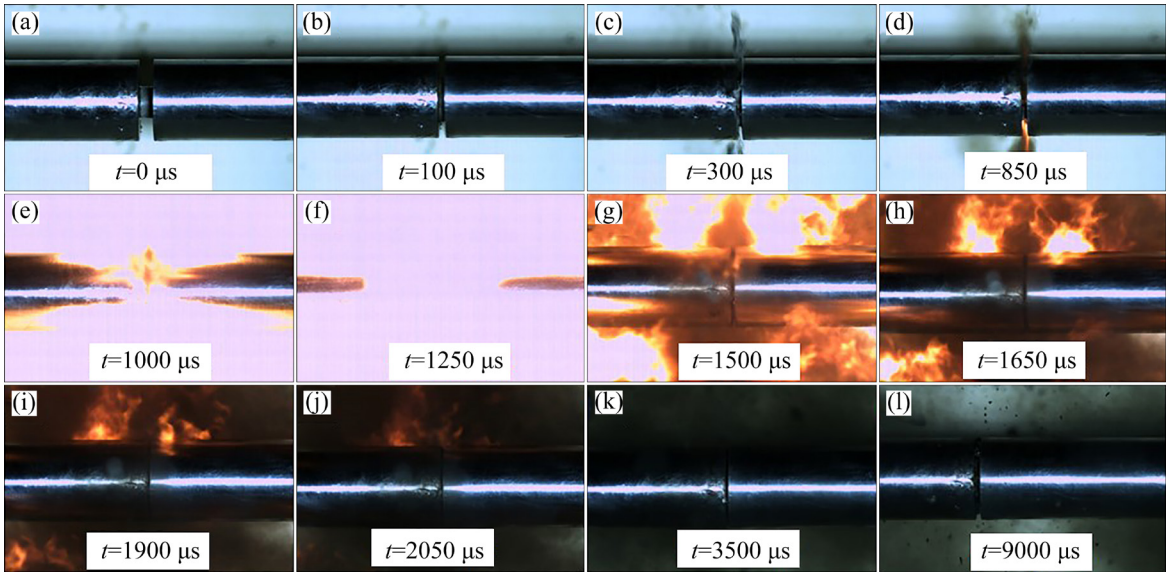

Fig. 8 Typical impact-initiation reaction processes of Type C at strain rate of 5000 s^{-1}

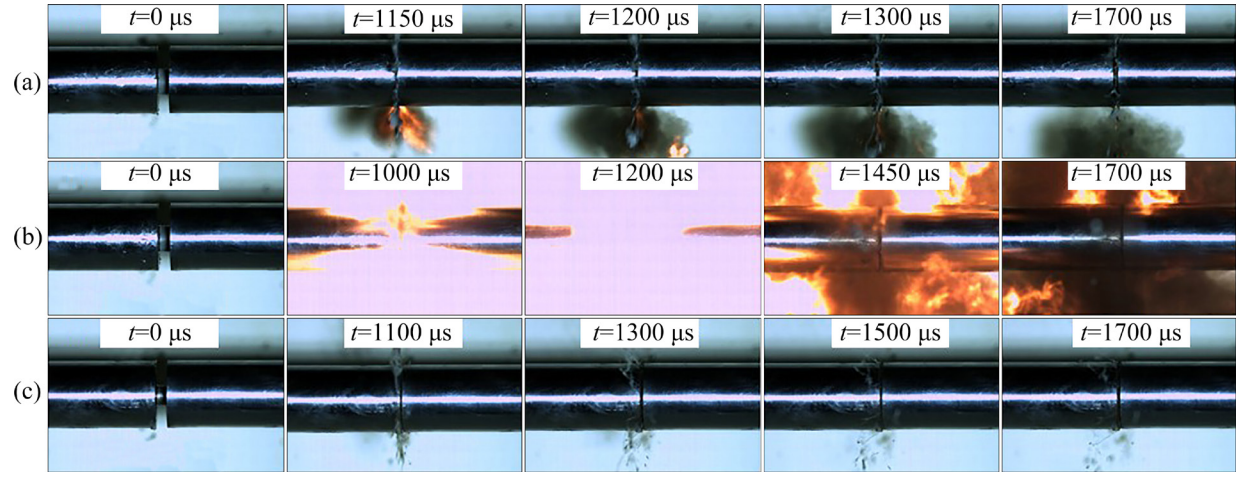

Fig. 9 Typical impact-initiation reaction processes of different types of specimens at strain rate of 5000 s^{-1}: (a) Type A; (b) Type C; (c) Type F

by [31]

$$E=\int_0^{\varepsilon_m}\sigma(\varepsilon)\mathrm{d}\varepsilon \quad (2)$$

where E is the strain energy, ε_m is the failure strain, σ is the stress, and ε is the strain. As seen from Eq. (2), the strain energy can be expressed by the area enclosed by the true stress−strain curves and the coordinate axis. In the case of sufficient impact ignition reaction, the calculated strain energy values according to true stress−strain curves in Fig. 7(c), at the strain rate of 5000 s^{-1}, are listed in Table 3. As seen from Table 3, with increase in Fe content, the dynamic compression strength and strain energy increased first and then decreased, which showed the similar trend of reactivity as shown in Fig. 9. In other words, the specimen with higher compression strength had higher reactivity because it absorbed more strain energy. A similar phenomenon was reported by FENG et al [3] and SWALLOWE and FIELD [32]. They observed that the specimens with higher toughness reacted more easily. Although the compression strength of Type C was lower than that of Type D, the specimen had higher reactivity, which was due to the fact that the reactivity was more than the absorbed strain energy.

3.3.4 Fitting of Johnson−Cook constitutive model

The Johnson−Cook (J−C) model is an empirical constitutive model based on a large amount of experimental data, which can simulate the mechanical response under high strain rate and high temperature loading. The model is described in detail in literature [33,34] and the equation is expressed as

$$\sigma=\left(A+B\varepsilon_p^n\right)\left[1+C\ln\left(\frac{\dot{\varepsilon}}{\dot{\varepsilon}_0}\right)\right]\left(1-T^{*m}\right) \quad (3)$$

where ε_p, $\dot{\varepsilon}$ and $\dot{\varepsilon}_0$ stand for plastic strain, strain rate and reference strain rate, respectively, and A, B, n, C and m are material constants. Since the tests were conducted at room temperature, the temperature softening effect of the materials can be ignored. Hence, the equation can be simplified as

$$\sigma=\left(A+B\varepsilon_p^n\right)\left[1+C\ln\left(\frac{\dot{\varepsilon}}{\dot{\varepsilon}_0}\right)\right] \quad (4)$$

Taking Type D as an example, the data obtained from SHPB tests were used to simulate the J−C equation. The fitting parameters are listed in Table 4, and the comparison between the fitting and experimental results is presented in Fig. 10. The final J−C model constitutive equation is as follows:

$$\sigma=\left(22.5+88.0003\varepsilon_p^{0.91768}\right)\left[1+0.20406\ln\left(\frac{\dot{\varepsilon}}{\dot{\varepsilon}_0}\right)\right] \quad (5)$$

Table 4 J−C model parameters obtained from SHPB tests at $\dot{\varepsilon}_0=1\times10^{-3}$ s^{-1}

Material constant	Fitting value	Standard error	R^2
A	22.5	0	1
B	88.0003	0.06223	0.99445
n	0.91768	0.00108	0.99445
C	0.20406	0.05135	0.83139

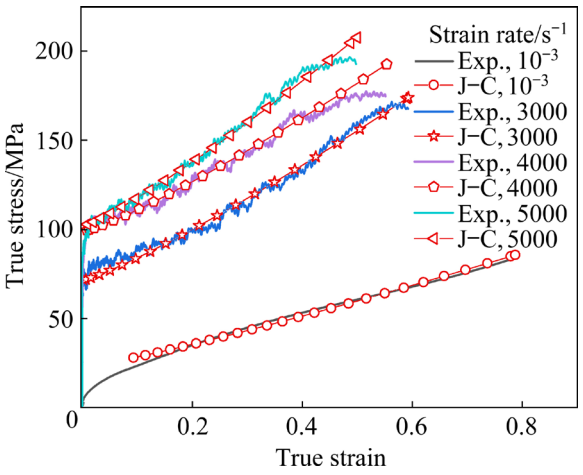

Fig. 10 Comparison between fitting and experimental results of Type D under different strain rates

As can be seen from Fig. 10, the fitting results were in good agreement with the experimental data, indicating that the established model could effectively describe the mechanical response at different strain rates. Considering the actual application scenarios of the specimens, such as reaction warheads, impact fragments and energetic liners, it is difficult to use experimental methods to study these high-speed impact behaviors. Therefore, the J−C model can be applied to effectively predicting the dynamic mechanical response and can provide a reference for practical applications.

3.4 Impact reaction characteristics under drop-weight tests

3.4.1 Impact sensitivity and reaction process analysis

The impact sensitivity of Al/PTFE/Fe composites was calculated according to Eq. (1). In

order to judge whether the reaction occurred and to record the reaction process, a high-speed camera was used. The impact sensitivity curves are shown in Fig. 11, and the related parameters are summarized in Table 5.

As can be seen from Table 5, with the increase in Fe content, impact sensitivity increased first and then decreased. When Fe content was 20%, the specimen was the most sensitive, which meant that Type C reacted more easily under the same impact conditions. Considering the mechanochemical initiation mechanism, the specimens with higher compression strength would have higher reactivity because they can absorb more mechanical work. Besides, the initiation of reaction has to overcome a certain barrier, which is referred to the apparent activation energy (E_a) [4]. The reactivity of Al with other oxidants is mainly related to its standard electrode potential. The more negative the electrode potential, the greater the free energy corresponding to the element and the higher the activity [5]. The electrode potentials of F and Fe^{3+} are −3.053 and −0.771 V, respectively, indicating that the reaction between Al and C_2F_4 is easier than that between Al and Fe. However, with the increase in Fe content, the compression strength increased but the reaction between Al and Fe gradually became dominant, which meant that the reaction needed to overcome more barriers. Based on the synergy of the two factors, Type C under the drop-weight conditions had the highest sensitivity.

Similar to the impact reaction process of SHPB, under the drop-weight conditions, Al/PTFE/Fe reactive materials would also be initiated and react violently. The reaction processes at the drop-weight height of 130 cm were recorded, as shown in Fig. 12. Taking Type C as an example, the results showed that the specimen underwent severe

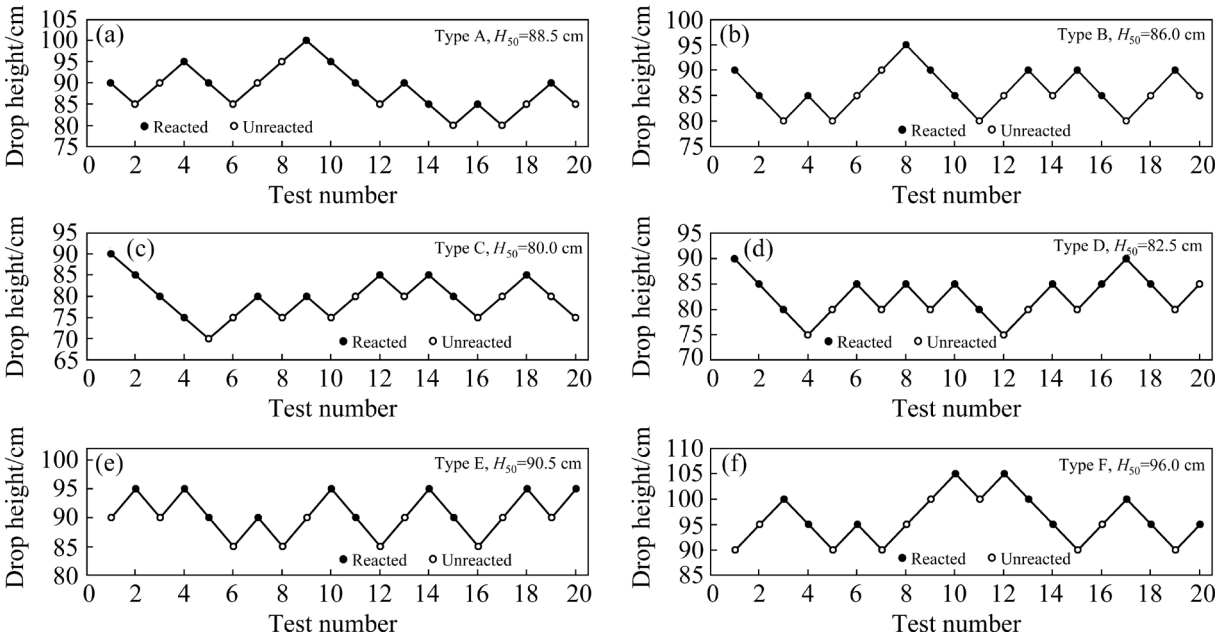

Fig. 11 Impact sensitivity curves of different types of specimen

Table 5 Impact reaction parameters of different specimens under drop-weight condition

Type	Characteristic drop-weight height, H_{50}/cm	Reaction delay time/μs	Reaction time/μs	Overpressure/ MPa	Piston motion time/ms
A	88.5	500	2600	0.089	1.64
B	86.0	500	2500	0.096	1.58
C	80.0	400	2400	0.161	1.31
D	82.5	450	2450	0.145	1.50
E	90.5	500	1000	0.072	1.82
F	96.0	550	700	0.061	2.03

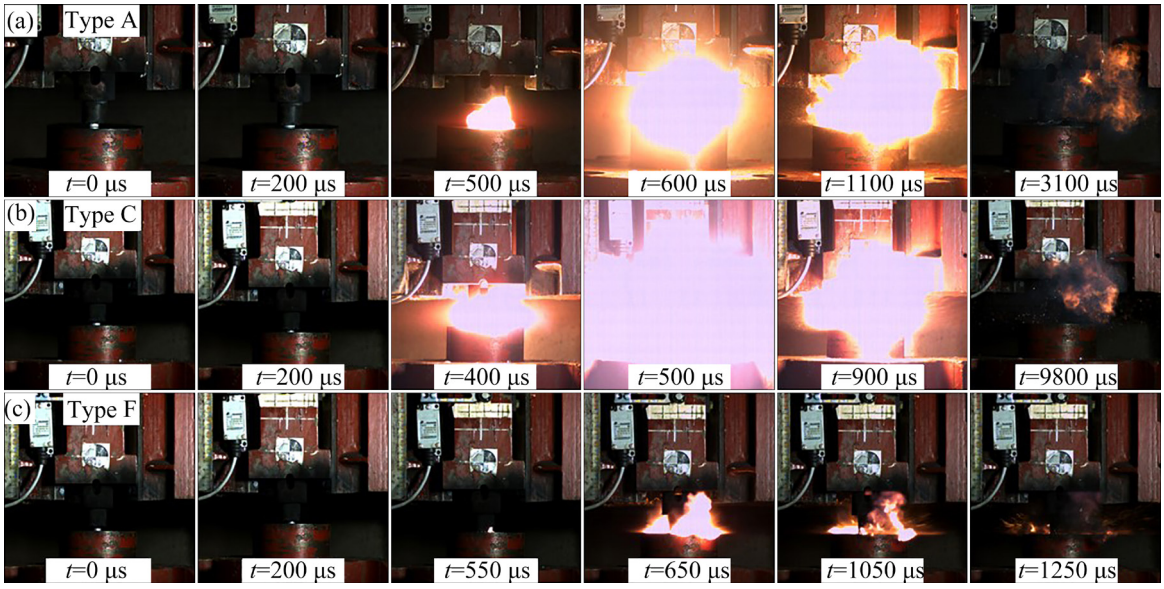

Fig. 12 Impact reaction processes of different types of specimens under drop-weight condition: (a) Type A; (b) Type C; (c) Type F

deformation upon impact loading (Fig. 12(b)). Soon after the deformation, the specimen failure occurred and some local scattered fragments and flame appeared. This indicated the formation of hot-spots and the initiation of the reaction, at t=400 μs. As the loading proceeded, more fragments took part in the reaction and the flame became brighter, which grew along the rebound direction of the drop-weight and burned out into a mushroom-like shape, at t=500−900 μs. Subsequently, the reaction gradually extinguished, and only some unreacted fragments splashed, at t=2800 μs. As shown in Table 5, when the Fe content increased, the reactivity increased first and then decreased. Type C had the shortest reaction delay time due to the change in impact sensitivity.

3.4.2 Quantitative energy release tests by newly designed drop-weight device

The impact reactivity judged by the flame size alone is inaccurate. Therefore, in order to qualitatively characterize the relationship between Fe content and impact energy release ability, the newly-designed drop-weight device described in Section 2.2.4 was used. The corresponding results are shown in Fig. 13.

As can be seen from Figs. 13(a) and Table 5, the overpressure value increased first and then decreased, reaching the maximum overpressure of 0.161 MPa with Fe content of 20%. The energy release ability characterized by overpressure was consistent with the previous results of flame size, but more accurate. Under the impact of drop-weight, the composites reacted violently and the piston pipe moved outward under the overpressure of chamber. As can be seen from the displacement-time curves (Fig. 13(b)) of the piston pipe, Type C needed the shortest time to move the same distance. Driven by the overpressure of chamber, the acceleration (a) of the piston was the largest, which meant that Type C had the highest energy release rate. By comparing the overpressure value and piston movement time (Fig. 13(c)), the overpressure value with Fe content of 20% was the largest, and the corresponding piston movement time was the shortest. The different test methods mutually verified that the experiment equipment and data were feasible and reliable, and Type C had the highest reactivity and reaction release rate. The impact reaction processes using the improved device are shown in Fig. 14. Under the overpressure of chamber, the piston pipe flew out of the guide sleeve, accompanied by splashing fire and a cloud of black smoke. Using the newly-designed drop-weight experiment device, the energy release effect with different Fe contents was qualitatively characterized for the first time.

3.5 Chemical reaction mechanism of composites

3.5.1 Thermal behavior under TG-DSC tests and XRD tests

In order to investigate the thermal reaction

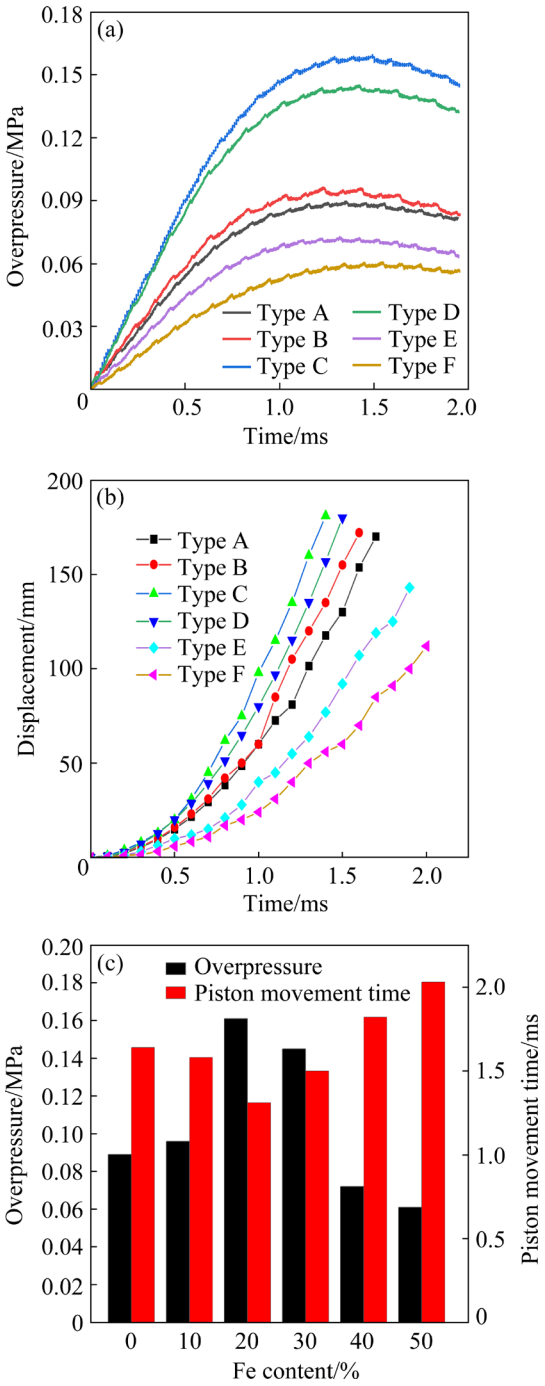

Fig. 13 Qualitatively energy release effect of different Al/PTFE/Fe reactive materials: (a) Overpressure−time curves; (b) Displacement−time curves of piston; (c) Histogram of overpressure and movement time

process of Al/PTFE/Fe composites, TG-DSC tests were carried out, and the results are shown in Fig. 15. Two endothermic peaks and one exothermic peak (two exothermic peaks in type C) were observed in the thermal decomposition process.

The endo-peak-A started at 310 °C, which was the melting endothermic peak of PTFE. During this

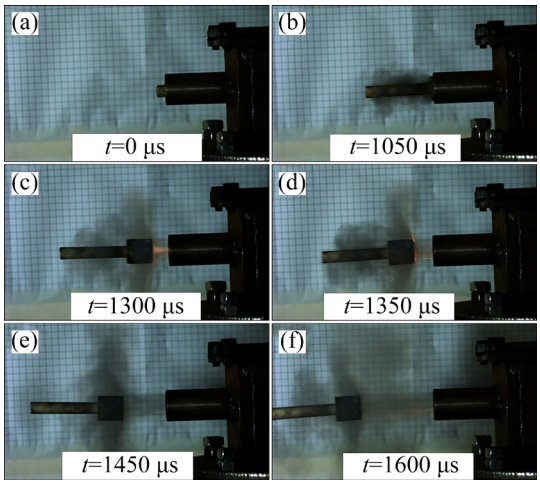

Fig. 14 Impact reaction process using newly-designed device of Type C

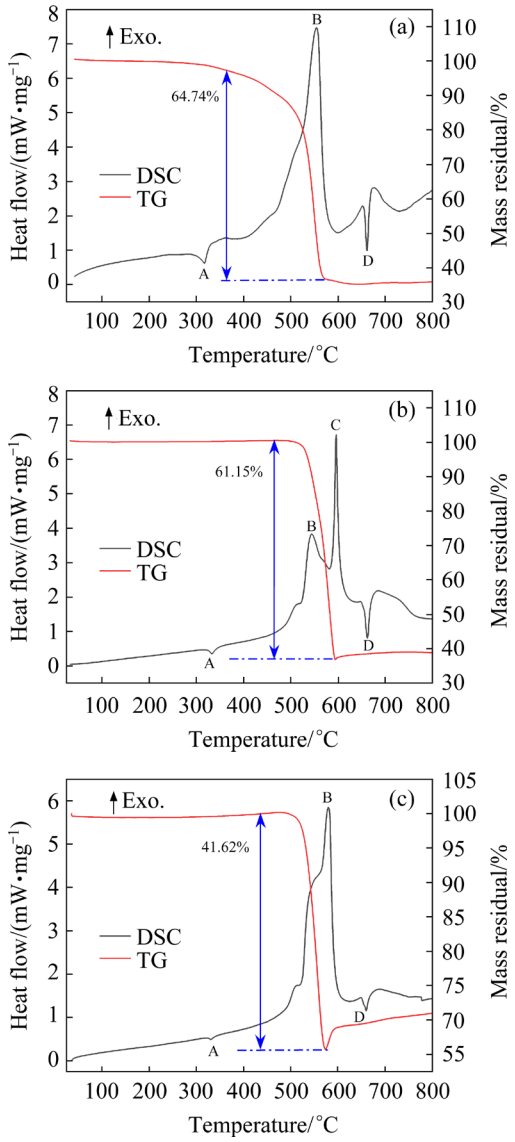

Fig. 15 TG-DSC curves of different types of specimens: (a) Type A; (b) Type C; (c) Type E

stage, the PTFE changed from crystalline to amorphous state and there was no mass loss in TG curves. The exo-peak-B started at 400 ℃ in Fig. 15(a), accompanied by a sharp decline in TG curves, which corresponded to the thermal decomposition of PTFE into gas C_2F_4 and the chemical reaction between Al and C_2F_4 [35]. The reaction heat was 1225 J/g. However, when Fe content was 20%, the exo-peak-B started at 400 ℃, and the reaction heat was 612 J/g, as shown in Fig. 15(b). After Peak B, another exo-peak-C appeared at 585 ℃, corresponding to the intermetallic reaction between Al and Fe [36,37]. The corresponding reaction heat was 210 J/g. As Fe content increased to 40%, the exothermic peaks between Al/PTFE and Al/Fe merged together, as shown in Fig. 15(c). This could be because excessive Fe powder acted as a dispersant and decreased the contact areas between Al and PTFE, causing the reaction temperature of Al/PTFE to shift backward. Since the reaction heat per unit mass of Al/Fe compound is lower than that of Al/PTFE, the entire reaction heat of the specimens decreased with the increase in Fe content. The endo-peak-D started at 650 ℃, which corresponded to the melting endothermic peak of unreacted Al powder. The detailed parameters of the exothermic Peaks B and C are listed in Table 6.

After TG-DSC tests, XRD tests were carried out to detect the reaction products and clarify the reaction process. Type C samples after sintering at 360, 550, 600 and 700 ℃ were collected and the residues were analyzed. The corresponding results are shown in Fig. 16. Before sintering, the composite was mainly composed of pure Al, Fe and $(C_2F_4)_n$ phases. After sintering at 360 ℃ for 5 h, the specimen only underwent a series of physical changes without the formation of new phases. Due to the decomposition of PTFE, the reaction between Al and PTFE occurred and the new phase of AlF_3 was formed, which was indicated by the residues collected after sintering at 550 ℃. However, there were also two low-intensity AlFe diffraction peaks in the pattern, which showed that the reactions between Al/PTFE and Al/Fe were not in a progressive order. They had similar reaction temperature ranges and a competing reaction may exist. After sintering at 600 ℃, which was after the exo-peak-C in Fig. 15(b), the phases were not changed, but the intensity of AlFe phase increased significantly. This result demonstrated that the diffusion rate and intermetallic compound reaction between Al and Fe powders were accelerated. After sintering at 700 ℃, the intensity of AlFe phase continued to increase. However, there was no diffraction peak of FeF_3 in the pattern, which showed that the reaction between Fe and gas $(CF_2)_n$ did not occur. According to the above results, the chemical reaction process may occur as follows:

$$\begin{cases} (-C_2F_4-)(s)\rightarrow(CF_2)_n(g),\ \Delta H=+1.71\ \text{kJ/g} \\ 4Al+3(-C_2F_4-)\rightarrow 4AlF_3+6C, \\ \quad \Delta H=-8.53\ \text{kJ/g} \\ Al+Fe\rightarrow AlFe,\ \Delta H=-0.606\ \text{kJ/g} \end{cases} \tag{6}$$

3.5.2 Initiation mechanism upon impact

Over the past few years, initiation mechanism has been extensively studied. AMES [19] proposed shear induced reaction mechanism using the Taylor impact tests, and observed that the hot-spots originated from the high-shear strain zone. ZHANG et al [38] used a quasi-sealed test chamber to study the impact response characteristics by varying the impact velocities, and proposed a thermochemical model which considered the reaction efficiency. The simulation results were consistent with the experimental results. FULLER et al [39] found that the impact velocity played a vital role. At impact velocities from 200 to 800 m/s, the elevated temperature at crack tips could reach 300−1000 ℃, which was high enough to initiate reaction.

Based on the above experimental results and

Table 6 Parameters of Peaks B and C of different types of materials

Type	Peak B			Peak C		
	Onset temperature/℃	Peak temperature/℃	Heat release/ ($J\cdot g^{-1}$)	Onset temperature/℃	Peak temperature/℃	Heat release/ ($J\cdot g^{-1}$)
A	400	556	1225	–	–	–
C	400	541	612	585	595	210
E	510	580	683	–	–	–

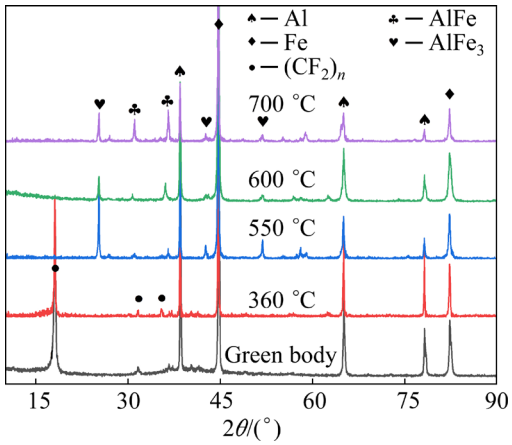

Fig. 16 XRD patterns of residues of Type C specimen at different temperatures

analyses, it is speculated that the initiation of reactive materials upon impact proceeds in a mechanochemical manner. When subjected to different strain rates, the specimens underwent an intense chemical reaction after they were completely broken, whether in drop-weight tests or in the SHPB tests. The specimens experienced severe plastic deformation during this stage. Moreover, due to the shear localization, mode-I open cracks formed, then the hot-spots formed at the crack tips and the reaction was triggered. It was inferred that the reactivity of Al/PTFE/Fe composites under dynamic impact was due to the multiple actions of uniformity of preparation, reaction heat of the specimen itself, absorbed strain energy, and the reaction initiation threshold. Besides, it was observed from fractured specimens in Fig. 5 that after plastic deformation, the constituents were laminated. There was also localized flow and sliding among the three constituents, which promoted the mixing of ingredients. This resulted in a reduction in the diffusion distance and further promoted the reaction. Furthermore, due to the high-speed impact and the rapidly propagating cracks, the surface impurities, especially inert alumina shell, were torn apart and the active aluminum was exposed, which promoted the reaction [3].

The mechanism of the formation of hot-spots varied with different materials and experimental conditions. Hence, the major formation mechanisms of hot-spots were summarized as follows: (1) Crack tips heating mechanism [40]: Under high-speed impact, the reactive materials undergo severe plastic deformation. Hence, a strong stress field is generated at the crack tips, resulting in the increase in temperature and formation of hot-spots. (2) Dislocation avalanche mechanism [41]: The dislocations in the strong shear strain area interact to release the energy of the dislocation band, and then generate hot-spots. (3) Bubble compression mechanism [42]: When the bubbles in the reaction material are compressed, they quickly heat up and form hot-spots. (4) Pore collapse mechanism [43]: When the impact waves propagate to the pores, the asymmetric collapse of the pores forms a jet stream, which generates heat and raises the local temperature, thereby forming the hot-spots. (5) Adiabatic shear mechanism [44]: The reactive materials undergo severe plastic deformation under impact loading, forming adiabatic shear bands. The friction at the surfaces of the particles increases the local temperature and forms hot-spots. The research on the formation mechanism of hot-spots also requires the application of new detection methods, such as thermocouple technology, infrared detection [45], and data modeling [46], which would be of great importance for the practical application of energetic materials.

4 Conclusions

(1) The specimens showed elasto-plastic characteristics. The compression strength reached the maximum of 108.5 MPa with Fe content of 30%, which was increased by 47.2% compared to Al/PTFE. Fractured surfaces were observed, and it was found that the oriented PTFE nano-fibers could prevent the propagation of cracks and increase the toughness of the composites.

(2) Dynamic compression tests were conducted by SHPB at elevated strain rates, and significant strain and strain rate hardening phenomena were observed. The compression strength reached 191.8 MPa at the strain rate of 5000 s^{-1} with the Fe content of 30%, which was increased by 39% compared to Al/PTFE. The Johnson−Cook constitutive model was fitted, which may provide a reference for engineering applications.

(3) Drop-weight tests were used to characterize material sensitivity, and the reactivity was qualitatively characterized for the first time by a newly-designed device. TG-DSC and XRD

analyses were conducted, which showed the decomposition of PTFE, Al and gaseous C_2F_4 reaction, and Al/Fe intermetallic reaction.

(4) Under impact loading, it was speculated that the impact initiation reaction occurred in a mechanochemical manner. The reactivity of Al/PTFE/Fe composites was likely due to the multiple actions of reaction heat of the material itself, absorbed strain energy and reaction initiation threshold. Besides, different formation mechanisms of hot-spots were summarized.

Acknowledgments

This work was supported by the Open Project of State Key Laboratory of Environment-friendly Energy Materials, China (No. 19kfgh07), R&D of Key Technology of Light Metal Air Battery, Transformation and Industrialization of Scientific and Technological Achievements of Hunan Province, China (No. 2020GK2071), and R&D of Key Technology and Materials of Magnesium Air Battery, Transformation of Scientific and Technological Achievements of Changsha City, China (No. Kh2005186).

References

[1] HE Wei, LIU Pei-jin, HE Guo-qiang, GOZIN M, YAN Qi-long. Highly reactive metastable intermixed composites (MICs): Preparation and characterization [J]. Advanced Materials, 2018, 30: e1706293.

[2] FENG Bin, FANG Xiang, LI Yu-chun, WANG Huai-xi, MAO Yi-ming, WU Shuang-zhang. An initiation phenomenon of Al−PTFE under quasi-static compression [J]. Chemical Physics Letters, 2015, 637: 38−41.

[3] FENG Bin, LI Yu-chun, WU Shuang-zhang, WANG Huai-xi, TAO Zhong-ming, FANG Xiang. A crack-induced initiation mechanism of Al−PTFE under quasi-static compression and the investigation of influencing factors [J]. Materials & Design, 2016, 108: 411−417.

[4] REN Hui-lan, LI Wei, NING Jiang-guo, LIU Yan-bin. The influence of initial defects on impact ignition of aluminum/polytetrafluoroethylene reactive material [J]. Advanced Engineering Materials, 2020, 22: 1900821−1900829.

[5] CAI J, WALLEY S M, HUNT R J A, PROUD W G, NESTERENKO V F, MEYERS M A. High-strain, high-strain-rate flow and failure in PTFE/Al/W granular composites [J]. Materials Science and Engineering A-Structural Materials Properties Microstructure & Processing, 2008, 472: 308−315.

[6] WANG Liu, LIU Jin-xu, LI Shu-kui, ZHANG Xin-bo. Investigation on reaction energy, mechanical behavior and impact insensitivity of W−PTFE−Al composites with different W percentage [J]. Materials and Design, 2016, 92: 397−404.

[7] XU Feng-yue, LIU Shu-bo, ZHENG Yuan-feng, YU Qing-bo, WANG Hai-fu. Quasi-static compression properties and failure of PTFE/Al/W reactive materials [J]. Advanced Engineering Materials, 2017, 19: 1600350−1600356.

[8] CAI J, NESTERENKO V F, VECCHIO K S, JIANG F, HERBOLD E B, BENSON D J, ADDISS J W, WALLEY S M, PROUD W G. The influence of metallic particle size on the mechanical properties of polytetraflouroethylene−Al−W powder composites [J]. Applied Physics Letters, 2008, 92: 031903−031906.

[9] HERBOLD E B, NESTERENKO V F, BENSON D J, CAI J, VECCHIO K S, JIANG F, ADDISS J W, WALLEY S M, PROUD W G. Particle size effect on strength, failure, and shock behavior in polytetrafluoroethylene−Al−W granular composite materials [J]. Journal of Applied Physics, 2008, 104: 103903−103913.

[10] WANG Huai-xi, LI Yu-chun, FENG Bin, HUANG Jun-yi, ZHANG Sheng, FANG Xiang. Compressive properties of PTFE/Al/Ni composite under uniaxial loading [J]. Journal of Materials Engineering and Performance, 2017, 26: 2331−2336.

[11] YU Zhong-shen, FANG Xiang, GAO Zhen-ru, WANG Huai-xi, HUANG Jun-yi, YAO Miao, LI Yu-chun. Mechanical and reaction properties of Al/TiH_2/PTFE under quasi-static compression [J]. Advanced Engineering Materials, 2018, 20: 1800019−1800024.

[12] WU Jia-xiang, HUANG Jun-yi, LIU Qiang, CHEN Yong, LI Yu-chun, YANG Li, YIN Qin, GAO Zhen-ru, WU Shuang-zhang, REN Xin-xin. Influence of ceramic particles as additive on the mechanical response and reactive properties of Al/PTFE reactive composites [J]. RSC Advances, 2020, 10: 1447−1455.

[13] DING Liang-liang, ZHOU Jin-yuan, TANG Wen-hui, RAN Xian-wen, HU Yu-xuan. Impact energy release characteristics of PTFE/Al/CuO reactive materials measured by a new energy release testing device [J]. Polymers, 2019, 11: 149−170.

[14] CAI Xiao-ping, LIU Ya-nan, FENG Pei-zhong, JIAO Xin-yang, ZHANG Lai-qi, WANG Jian-dong. Fe−Al intermetallic foam with porosity above 60% prepared by thermal explosion [J]. Journal of Alloys and Compounds, 2018, 732: 443−447.

[15] GAO Hai-yan, HE Yue-hui, ZOU Jin, XU Nan-ping, LIU C T. Tortuosity factor for porous FeAl intermetallics fabricated by reactive synthesis [J]. Transactions of Nonferrous Metals Society of China, 2012, 22: 2179−2183.

[16] ZHOU Jin-yuan, DING Liang-liang, TANG Wen-hui, RAN Xian-wen. Experimental study of mechanical properties and impact-induced reaction characteristics of PTFE/Al/CuO reactive materials [J]. Materials, 2019, 13: 66−83.

[17] WANG Hai-fu, GENG Bao-qun, GUO Huan-guo, ZHENG Yuan-feng, YU Qing-bo, GE Chao. The effect of sintering and cooling process on geometry distortion and mechanical properties transition of PTFE/Al reactive materials [J]. Defence Technology, 2020, 16: 720−730.

[18] GE Chao, MAIMAITITUERSUN W, DONG Yong-xiang, TIAN Chao. A study on the mechanical properties and

impact-induced initiation characteristics of brittle PTFE/Al/W reactive materials [J]. Materials, 2017, 10: 452−466.

[19] AMES R G. Energy release characteristics of impact-initiated energetic materials [J]. MRS Proceeding, 2005, 896: 896-H03.

[20] LIU Ya-nan, CAI Xiao-ping, SUN Zhi, ZHANG Han-zhu, AKHTAR F, CZUJKO T, FENG Pei-zhong. Fabrication and characterization of highly porous FeAl-based intermetallics by thermal explosion reaction [J]. Advanced Engineering Materials, 2019, 21: 1801110−1801119.

[21] WANG Qian, LENG Xue-song, YANG Tian-hao, YAN Jiu-chun. Effects of Fe−Al intermetallic compounds on interfacial bonding of clad materials [J]. Transactions of Nonferrous Metals Society of China, 2014, 24: 279−284.

[22] HUANG Jun-yi, FANG Xiang, WU Shuang-zhang, YANG Li, YU Zhong-sheng, LI Yu-chun. Mechanical response and shear-induced initiation properties of PTFE/Al/MoO_3 reactive composites [J]. Materials, 2018, 11: 1200−1213.

[23] XIONG Wei, ZHANG Xian-feng, WU Yang, HE Yong, WANG Chuang-ting, GUO Lei. Influence of additives on microstructures, mechanical properties and shock-induced reaction characteristics of Al/Ni composites [J]. Journal of Alloys and Compounds, 2015, 648: 540−549.

[24] WEI C T, VITALI E, JIANG F, DU S W, BENSON D J, VECCHIO K S, THADHANI N N, MEYERS M A. Quasi-static and dynamic response of explosively consolidated metal-aluminum powder mixtures [J]. Acta Materialia, 2012, 60: 1418−1432.

[25] FENG Bin, QIU Cong-li, ZHANG Tao-hong, HU Ya-feng, LI Hong-guang, XU Bing-chuan. Sensitivity of Al-PTFE upon low-speed impact [J]. Propellants Explosives Pyrotechnics, 2019, 44: 630−636.

[26] BROWN E N, DATTELBAUM D M. The role of crystalline phase on fracture and microstructure evolution of polytetrafluoroethylene (PTFE) [J]. Polymer, 2005, 46: 3056−3068.

[27] KITAMURA T, OKABE S, TANIGAKI M, KURUMADA K, OHSHIMA M, KANAZAWA S I. Morphology change in polytetrafluoroethylene (PTFE) porous membrane caused by heat treatment [J]. Polymer Engineering & Science, 2000, 40: 809−817.

[28] TANG En-ling, LI Sheng, CHEN Chuang, HAN Yan-fei. Dynamic compressive behavior of fiber reinforced Al/PTFE active materials [J]. Journal of Materials Research and Technology, 2020, 9: 8391−8400.

[29] JIE M, TANG C Y, LI Y P, LI C C. Damage evolution and energy dissipation of polymers with crazes [J]. Theoretical and Applied Fracture Mechanics, 1998, 28:165−174.

[30] ZHANG Xian-feng, ZHANG Jun, QIAO Lin, SHI An-shun, ZHANG Yu-gan, HE Yu, GUAN Zhi-wen. Experimental study of the compression properties of Al/W/PTFE granular composites under elevated strain rates [J]. Materials Science and Engineering A-Structural Materials Properties Microstructure and Processing, 2013, 581: 48−55.

[31] LI Yan, WANG Zai-cheng, JIANG Chun-lan, NIU Hao-hao. Experimental study on impact-induced reaction characteristics of PTFE/Ti composites enhanced by W particles [J]. Materials, 2017, 10: 175−187.

[32] SWALLOWE G M, FIELD J E. The ignition of a thin layer of explosive by imapact−The effect of polymer particles [J]. Proceedings of the Royal Society of London, Series A: Mathematical and Physical Sciences, 1982, 379: 389−408.

[33] JOHNSON G R, COOK W H. A constitutive model and data for metals subjected to large strains, high strain rates and high temperatures [J]. Engineering Fracture Mechanics, 1983, 21: 541−548.

[34] SVOBODA R, MÁLEK J. Applicability of Fraser−Suzuki function in kinetic analysis of complex crystallization processes [J]. Journal of Thermal Analysis and Calorimetry, 2013, 111: 1045−1056.

[35] YU Zhong-shen, LI Yu-chun, GUO Tao, ZHANG Jun, WU Shuang-sheng, HUANG Jun-yi, SONG Jia-xing, FANG Xiang. Chemical reaction mechanism and mechanical response of PTFE/Al/TiH_2 reactive composites [J]. Journal of Materials Engineering and Performance, 2019, 28: 7493−7501.

[36] CAI Xiao-ping, LIU Ya-nan, WANG Xiao-hong, JIAO Xin-yang, WANG Jian-zhong, AKHTAR F, FENG Pei-zhong. Oxidation resistance of highly porous Fe−Al foams prepared by thermal explosion [J]. Metallurgical and Materials Transactions A—Physical Metallurgy and Materials Science A, 2018, 49(8): 3683−3691.

[37] YANG Ming, MA Hong-Hao, SHEN Zhao-wu, CHEN Dai-guo, DENG Yong-xin. Microstructure and mechanical properties of Al−Fe meshing bonding interfaces manufactured by explosive welding [J]. Transactions of Nonferrous Metals Society of China, 2019, 29: 680−691.

[38] ZHANG Xian-feng, SHI An-shun, QIAO Li, ZHANG Jun, ZHANG Yu-gan, GUAN Zhi-wen. Experimental study on impact-initiated characters of multifunctional energetic structural materials [J]. Journal of Applied Physics, 2013, 113: 083508−083518.

[39] FULLER K N G, FOX P G, FIELD J E. The temperature rise at the tip of fast-moving cracks in glassy polymers [J]. Proceedings of the Royal Society A, 1975, 341: 537−557.

[40] YU C , PANDOLFI A , ORTIZ M, COKER D, ROSAKIS A J. Three-dimensional modeling of intersonic shear-crack growth in asymmetrically loaded unidirectional composite plates [J]. International Journal of Solids and Structures, 2002, 39: 6135−6157.

[41] SMALLWOOD J M, FIELD J E. Hot-spot ignition mechanisms for explosives and propellants [J]. Philosophical Transactions of the Royal Society A, 1992, 339: 269−283.

[42] MILNE A M, BOURNE N K. Experimental and numerical study of temperatures in cavity collapse [C]//Proc Shock Compression of Condensed Matter 2001. Atlanta, GA: TMS, 2001, 620: 914−917.

[43] CHAUDHRI M M, FIELD J E. The role of rapidly compressed gas pockets in the initiation of condensed explosives [J]. Proceedings of the Royal Society A: Mathematical, 1974, 10: 1−6.

[44] KANG J, BUTLER P B, BAER M R. A thermomechanical analysis of hot spot formation in condensed-phase, energetic materials [J]. Combustion and Flame, 1992, 89: 117−139.

[45] REN Ke-rong, CHEN Jin, QING Hua, CHEN Rong, CHEN Peng, LIN Yu-liang, GUO Bao-yue. Study on shock-induced

chemical energy release behavior of Al/W/PTFE reactive material with mechanical-thermal-chemical coupling SPH approach [J]. Propellants Explosives Pyrotechnics, 2020, 45: 1937−1948.

[46] GUO Bao-yue, REN Ke-rong, LI Zhi-bin, CHEN Rong. Modelling on shock-induced energy release behavior of reactive materials considering mechanical-thermal-chemical coupled effect [J]. Shock and Vibration, 2021, 2021: 1−12.

Fe 颗粒增强 Al/PTFE 反应材料的力学性能、冲击反应特性及能量释放效应

项向春[1]，张青春[2]，房洪杰[1,3]，郭宝月[4]，梁 文[4]，金 波[2]，彭汝芳[2]，余 琨[1]，陈 荣[4]

1. 中南大学 材料科学与工程学院，长沙 410083；
2. 西南科技大学 环境友好能源材料国家重点实验室，绵阳 621010；
3. 烟台南山学院 材料科学与工程学院，烟台 265713；
4. 国防科技大学 理学院，长沙 410008

摘 要：铝/聚四氟乙烯(Al/PTFE)复合材料是一种非常有前景的反应结构材料。为了提高材料的力学性能和反应性，将 Fe 颗粒加入 Al/PTFE 反应材料中。对 Al/PTFE/Fe 反应材料进行准静态和动态压缩试验，观察到明显的应变和应变率硬化现象，且当 Fe 含量为 30%(质量分数)时，在 5000 s^{-1} 的应变率下，抗压强度达 191.8 MPa，较 Al/PTFE 提升了 39%。定向的 PTFE 纳米纤维丝能有效地阻碍裂纹的扩展。通过高速摄影对霍普金森杆和落锤冲击下的能量释放进程进行观察，且通过新设计的装置对反应活性进行定量表征。结合 TG-DSC 和 XRD，明确了 Al/PTFE 和 Al/Fe 之间的反应。通过霍普金森杆的实验数据建立 Johnson−Cook 本构模型，模型结果与实验数据吻合较好。在冲击状况下，材料的反应性是多重行为的结果。

关键词：反应材料；铝/聚四氟乙烯/铁(Al/PTFE/Fe)；力学性能；能量释放特征；冲击引发机理

(Edited by Xiang-qun LI)